Tellus (1986), *38A*, 251–262

Topographically-induced mesoscale motions in antitriptically balanced barotropic flow

By WILLIAM H. RAYMOND, *Department of Meteorology, The University of Wisconsin, 1225 West Dayton Street, Madison, Wisconsin 53706, USA.*

(Manuscript received February 12; in final form September 5, 1985)

ABSTRACT

The dynamic processes within a steady viscous incompressible barotropic fluid interacting with an isolated mesoscale obstacle are studied. The topography is allowed to disrupt a variety of antitriptically balanced background states. Localized forcing and damping results when the mean balanced state is upset. A mesoscale antitriptic pressure gradient of a trough (ridge) is shown to enhance lee-side confluence if positioned just upstream (downstream) of the topographical center. Repositioning the trough (ridge) downstream (upstream) yields solutions similar to those obtained with an enhanced frictional drag. Comparisons are made against solutions obtained from calculations with constant frictional drag under mesoscale flow conditions, i.e., the Rossby number is near unity.

1. Introduction

The disruption of the airflow by major mountains is well-known. As an air parcel approaches such an obstacle its velocity is altered by the orographically disturbed horizontal pressure gradient (Smith, 1982). High pressure on the windward side divides the flow to the left and right and for major mountains the velocities are further modified by the Coriolis force. The resulting flow has a strong left–right asymmetry. On the other hand, it is known that friction produces an upstream–downstream asymmetry as has been demonstrated by Buzzi and Tibaldi (1977) and Bannon (1980). Both of these properties can be demonstrated from conceptually simple barotropic or depth averaged models, for examples of this technique see Lavoie (1974), Keyser and Anthes (1977), for mesoscale flow Han et al. (1982) and Bannon (1980) for large-scale flow (small Rossby number).

Generally in these slab models friction is characteristically introduced by utilizing a bulk aerodynamic formulation to parameterize the total surface stress in terms of a barotropic surface drag. The surface stress at the top of the surface layer or bottom of the mixed layer in reality varies according to the state of the lower troposphere. Mesoscale phenomena like cold fronts and squall lines characteristically have pre-storm environments where the lower troposphere is convectively unstable while the post-storm environment is relatively stable. It is well-known that stratification effects can cause substantial changes in some surface layer parameters. Horizontal variations in the baroclinic velocity fields, i.e., the height dependent velocities, on the mesoscale likewise add significant additional complications. Observations (Hoxit, 1974) and numerical models, e.g., (Keyser and Anthes, 1982), both show an enhanced (reduced) ageostrophic wind component directed toward low pressure in cold (warm) air advection. This horizontal variation in the flow in turn modifies the surface stress profile from those expected under barotropic conditions. Furthermore, frontal cyclones crossing a mountain range undergo some changes in structure (Barry, 1981). Consequently it is difficult to specify what surface layer characteristics should be present in these frontal situations. If these were known then a more complete depth averaged or barotropic solution could be computed.

In numerical experiments with and without the

Alps topography. Tibaldi et al. (1983) and Tosi et al. (1983) have both noted that the barotropic contribution to the kinetic energy is reduced for the cases containing the topography, once the low-level cold front nears the top of the alpine feature. A small enhancement in kinetic energy, however, occurs at low levels just prior to this general decline (Tibaldi et al., 1980). McGinley's (1982) study of lee cyclogenesis cases indicate that the conversion from mean to perturbation kinetic energy by barotropic and baroclinic mechanisms are significant just as the front impinges the lee slopes. Yet the contribution and importance of the barotropic process in encouraging a complicated event like lee cyclogenesis is difficult to distinguish and separate from the baroclinic process. To help with this identification and separation we will isolate the role of the barotropic process in this study. This in no way should be interpreted as minimizing the role of the baroclinic effects in frontal cyclone modification and in lee cyclogenesis.

Kalney-Rivas and Merkine (1982) and Pierrehumbert and Malguzzi (1984), investigating the blocking phenomena, have both shown that weak localized forcing (500–2000 km in scale) of non-linear barotropic flows can yield unexpected high amplitude responses significantly altering the initial synoptic zonal flows. This occurs for both f-plane and beta plane approximations, while as expected, the linearized version yields a low amplitude response (Pierrehumbert and Malguzzi, 1984). These authors indicate that for the high amplitude response case the prescribed localized vorticity forcing is balanced, in an averaged sense, by the Ekman friction while in the low amplitude (linear) case the sum of the imbalance remains bounded.

In this study we will concentrate on linear barotropic flow as a first step in understanding the origin of and the mesoscale response to localized forcing and damping. It will be shown that internally generated damping and forcing of the flow occurs when an isolated mesoscale topographical feature disrupts zonal flow in geostrophic and antitriptic balance. The latter represents, in the undisturbed state, a balance between the horizontal gradient of pressure and the vertical component of friction (analogous to Poiseuille flow). The forcing is not specified a priopri but results because of the internal coupling between the flow and the topography. The nature of this forcing for different mesoscale antitriptic states will be examined, e.g., an antitriptic pressure trough or ridge positioned on the upwind or downwind side of the topography.

An Oseen approximation (Stevensen and Janowitz, 1977) is utilized to find, as economically as possible, the steady-state solutions for viscous and/or forced barotropic flow from a boundary value approach. This technique yields accurate solutions provided the flow does not possess excessive curvature. This is indeed the case for mesoscale circulations having Rossby numbers near unity. Steady state solutions are deemed appropriate provided the antitriptic pressure trough or ridge is quasi-steady and stationary. Han et al. (1982) have shown that patterns induced by terrain are quickly attained and stable under external conditions provided the ratio of the magnitudes of the advection to the external surface stress terms are not large. To make use of the Oseen approximation, our equations are linearized; consequently we cannot examine the phenomenon of the hydraulic jump which arises only from non-linear equations (Houghton and Kasahara, 1968).

2. The mathematical model

The dynamic processes within a rotating incompressible viscous barotropic fluid are studied for flows over an isolated topographical feature. According to Bannon (1980) under conditions when the fluid is shallow and the Ekman number non-zero the governing equations obtained by depth averaging the Navier–Stokes equations, when expressed in terms of barotropic and baroclinic components, may be written for a beta plane approximation in terms of non-dimensional variables as

$$\varepsilon \frac{\mathrm{d}u}{\mathrm{d}t} - (1 + \hat{\beta}\varepsilon y)\, v = -\frac{\partial p}{\partial x} + \frac{E_k}{D} \frac{\partial u'}{\partial Z}\bigg|_{Z=\mu b}^{1+\lambda\varepsilon p}, \tag{1}$$

$$\varepsilon \frac{\mathrm{d}v}{\mathrm{d}t} + (1 + \hat{\beta}\varepsilon y)\, u = -\frac{\partial p}{\partial y} + \frac{E_k}{D} \frac{\partial v'}{\partial Z}\bigg|_{Z=\mu b}^{1+\lambda\varepsilon p}, \tag{2}$$

$$\frac{\mathrm{d}D}{\mathrm{d}t} + D\left(\frac{\partial u}{\partial x} + \frac{\partial v}{\partial y}\right) = 0, \tag{3}$$

where the fluid is of depth $D = 1 + \lambda\varepsilon p - \mu b$ and $\mathrm{d}/\mathrm{d}t = \partial/\partial t + u\, \partial/\partial x + v\, \partial/\partial y$. The last term in eqs. (1) and (2) represent the net contribution of the upper and lower baroclinic surface stresses where the depth averaging is performed between the top of the barotropic layer at $Z = 1 + \lambda \varepsilon p$ and the top of the surface layer at $Z = \mu b$. The depth averaged layer plus surface layer has a total thickness of $Z^* = Z + \delta$, where the surface layer depth is δ and is taken as a constant. Here u, v and u', v' are the barotropic and baroclinic horizontal velocities in the x and y coordinate directions respectively, t is time and p is the depth-averaged pressure. The parameters ε, λ, and E_k represent the Rossby, the rotational Froude and the Ekman numbers while $\hat{\beta}$ is the variation of the dimensionless Coriolis parameter in the y direction. Mesoscale characteristic values of length scale L about 10^5 m, height scale H near 3×10^3 m and velocity scale U about 10 m s^{-1} yields values for these parameters of around $\varepsilon \approx 1$, $\lambda \approx 0.1$ and $\hat{\beta} \approx 10^{-2}$ while we assume $E_k < 1$. The topographical parameter μ is taken to be a significant fraction of the mean fluid depth. The mesoscale topographical feature centered at $x = y = 0$ is assigned the Gaussian horizontal shape prescribed by

$$b(x, y) = \exp\left\{-a\left[\left(\frac{x}{\sigma_x}\right)^2 + \left(\frac{y}{\sigma_y}\right)^2\right]\right\}. \tag{4}$$

We assign $a = \ln 2$ and $\sigma_x = \sigma_y = 1$ so that the value of b falls to half its maximum in one unit of non-dimensional horizontal distance and is circularly symmetric and possesses continuous derivatives. The formulation of the equations assumes hydrostatic flow since the horizontal scale of the topographically induced motion greatly exceeds the fluid depth. Also no horizontal viscosity is included. In this study the surface stress at the top of the barotropic layer is ignored so as to better concentrate on the contribution from the surface stress at the bottom of the layer. Actually both can be important.

Eqs. (1)–(3) with assigned parameters forms a closed system for the dependent variables u, v and D provided the baroclinic surface stress terms are known. If these stresses are independent of the barotropic flow they would represent pure external forcing terms. Mahrt (1974) indicates that a coupling is necessary, however, for finite time steady depth averaged solutions to exist. Under neutral conditions the lower surface acts as a drag. Mahrt (1974) indicates the surface stress will generally be to the left of the layer averaged winds, however, baroclinity greatly changes the situation.

Our approach is to apply the Taylor (1915) geophysical boundary condition to the total wind components $u_T = u + u'$ and $v_T = v + v'$ so that

$$k \frac{\partial u_T}{\partial Z^*} = u_T, \tag{5a}$$

$$k \frac{\partial v_T}{\partial Z^*} = v_T, \tag{5b}$$

where k is to be determined. Eqs. (5a,b) are valid in the surface layer and k is a function of location (x, y), height $Z^* = \delta$ and stability.

Substituting from the surface layer solutions obtained from similarity theory for u_T and v_T (e.g. see Haltiner and Williams, 1980) into eqs. (5a,b) and solving for k yields

$$k(x, y) = [\ln Z^*/Z_0 - \psi'] \left[Z^{*-1} - \frac{d\psi'}{dz}\right]^{-1}\Bigg|_{Z^* = \delta}, \tag{5c}$$

where Z_0 is a surface roughness height and ψ' is a stability factor dependent on the mixing length scale. It is to be noted that the expression for k is identical in eqs. (5a,b) and it is independent of the von Karman constant, a friction velocity or a cross isobar flow angle. The horizontal variation of k however is not known unless the variation of ψ' with respect to x and y is known. For neutral stability eqs. (5) reduces to the conditions used for the boundary layer winds in Kurihara and Bender (1983).

Since u is not a function of Z we simplify eqs. (5a) so that at the top of the surface layer

$$\frac{\partial u'}{\partial Z^*} = k^{-1}(1 + g_1)u \equiv K_1 u, \tag{5d}$$

provided k^{-1} exists and $u' = g_1 u$ if u is non-zero. Substituting for u_T in the standard surface layer governing equation† yields $\partial^2 g_1/\partial Z^{*2} + [\partial (\ln k^*)/\partial Z^*]\ \partial g_1/\partial Z^* = 0$, for viscosity k^*. The boundary conditions for g_1 are $\partial g_1/\partial Z^* = k^{-1}(1 + g_1)$ at $Z^* = \delta$ and $g_1(Z_0) = -1$. Similar expressions can be written relating v' and v. Not knowing k implies we can not solve for g_1, so it is necessary to have the baroclinic solutions or make some simplifying assumptions.

† $\partial(k^* \partial u_T/\partial Z^*)/\partial Z^* = 0$

In areas of localized convergence and divergence the baroclinic surface stress can actively either force or dampen the barotropic components. In the absence of baroclinic solutions it is still expedient to investigate the barotropic response to localized forcing as proposed by Pierrehumbert and Malguzzi (1984). It will be shown that forcing and damping exist when a fluid in geostrophic and antitriptic balance is disrupted by topography. In the absence of topography, or at minus infinity, the basic state is assumed to be in antitriptic balance, be geostrophic and zonal ($v = 0$) so that

$$0 = -\frac{\partial P_0}{\partial x} - E_k D^{-1} K_1 u, \tag{6a}$$

$$(1 + \hat{\beta}\varepsilon y)u = -\frac{\partial p}{\partial y}, \tag{6b}$$

and the fluid is of constant depth. Note that the balanced flow regime is satisfied by

$$u = 1, \quad v = 0, \quad D = 1, \quad \psi = -y,$$
$$K_1 = -E_k^{-1}\,\partial P_0/\partial x, \tag{6c–h}$$
$$p = -(y + \tfrac{1}{2}\hat{\beta}\varepsilon y^2).$$

The known pressure P_0 is taken to be a function only of x, i.e., perpendicular to a straight north–south trough or ridge and is understood to be that function of the mesoscale pressure whose gradient is balanced against the baroclinic surface stress. In the present formulation this pressure gradient is a function of one dimension only so no information is gleaned with regards to the other component of the surface stress. For convenience we replace $\partial v'/\partial Z^*$ with $K_2 v$ and test a number of situations, e.g., $K_2 = 0$, a constant, etc.

The antitriptic pressure gradient is hypothetically taken as

$$\frac{\partial P_0}{\partial x} = a - b(x - x_c)\,[1 + (x - x_c)^4]^{-1}, \tag{7}$$

where a, b and x_c are constants. From (7), it is easy to show in the balanced state, eqs. (6a,b,g) and eq. (5), that when v' is not a function of x or y then there is no baroclinic vertical component of relative vorticity in the surface layer, and there is baroclinic convergence when $|x - x_c| \leqslant 0.7598$ and weaker divergence when $|x - x_c| > 0.7598$ and this convergence or divergence is found to increase linearly with height within the surface layer. For the choices of a and b used, the dimensional pressure, defined by $p^* = \rho v f L P_0$, where ρ is the density and f the Coriolis parameter, yields magnitudes no larger than one-half a millibar over a length L. When ignoring the constant a in eq. (7) we note that for $b > 0$ the integrated solution for P_0 represents a weak mesoscale symmetric trough centered about x_c while $b < 0$ yields a mesoscale ridge. As with the topography the pressure falls to half its maximum value in one non-dimensional horizontal unit of distance.

From eqs. (1)–(3) and (5d) for the case of a β-plane and for steady flow, we form the vorticity and energy equations, given respectively by

$$\frac{1}{D} J\left(\psi, \frac{1 + \hat{\beta}\varepsilon y + \varepsilon\zeta}{D}\right) = -\frac{E_k}{D}\frac{\partial}{\partial x}\left(\frac{K_2 v}{D}\right) + \frac{E_k}{D}\frac{\partial}{\partial y}\left(\frac{K_1 u}{D}\right), \tag{8a}$$

$$J\left(\psi, \frac{u^2 + v^2}{2} + \frac{1}{\lambda\varepsilon^2} + \frac{p}{\varepsilon}\right) = -\varepsilon^{-1}\left[u\frac{\partial P_0}{\partial x} - \frac{E_k}{D}(K_1 u^2 + K_2 v^2)\right]. \tag{8b}$$

The vertical component of vorticity ζ and the velocity components u and v are expressed in terms of the streamfunction ψ, via,

$$\zeta = v_x - u_y = D^{-1}[\nabla^2\psi - D^{-1}(\psi_x D_x + \psi_y D_y)], \tag{9a}$$

$$u = -D^{-1}\psi_y, \tag{9b}$$

$$v = D^{-1}\psi_x. \tag{9c}$$

Here J is the Jacobian operator, $J(S, R) = -S_y R_x + S_x R_y$, and ∇^2 is the Laplacian operator and the subscripts denote partial differentiation.

Eqs. (8a) and (8b) are coupled provided the rotational Froude number λ is non-zero. Under mesoscale conditions and mountains the values of both λ and $\hat{\beta}$ are, however, small and consequently have a restrained influence. Limiting our investigation to pure rotational flow in hydrostatic balance is consistent with assigning these parameters zero (see ch. 3, Haltiner and Williams (1980)). Under these conditions uncoupling eqs. (8a) and (8b) by replacing the upper free boundary with a rigid lid ($\lambda = 0$) appears justified.

For the case when $P_0 = 0$ and/or $K_1 = K_2 = 0$ the right side is zero and the method of solution is given in Charney (1955). Provided there are no closed streamlines and taking note that eqs. (8a,b) are decoupled ($\lambda = 0$ case only) we can write

$$[1 + \hat{\beta}\varepsilon y + \varepsilon\zeta]D^{-1} = F(\psi), \tag{10a}$$

$$\frac{u^2 + v^2}{2} + \varepsilon^{-1} p = G(\psi), \tag{10b}$$

where

$$F(\psi) = F(\psi_\infty), \tag{11a}$$

$$G(\psi) = G(\psi_\infty), \tag{11b}$$

and the upstream flow conditions (6c–h) are satisfied. Consequently $\zeta = 0$ and

$$F(\psi) = 1 - \hat{\beta}\varepsilon\psi, \tag{12a}$$

$$G(\psi) = \tfrac{1}{2} + \varepsilon^{-1}(\psi - \tfrac{1}{2}\hat{\beta}\varepsilon\psi^2). \tag{12b}$$

Solving for the vorticity ζ in eq. (10a) and for the pressure p in eq. (10b), utilizing (12a) and (12b) respectively, yields

$$\zeta = -\hat{\beta}(\psi + y) - \mu b\left(\frac{1}{\varepsilon} - \hat{\beta}\psi\right), \tag{13a}$$

$$p = \psi - \tfrac{1}{2}\hat{\beta}\varepsilon\psi^2 + \varepsilon[\tfrac{1}{2} - \tfrac{1}{2}(u^2 + v^2)]. \tag{13b}$$

For a viscous fluid additional terms must be added to these expressions. We utilize an Oseen approximation, as advocated by Huppert and Stern (1974) and Stevenson and Janowitz (1977), and linearize about $u = 1$ and $v = 0$ and then integrate with respect to x yielding

$$\zeta = -\hat{\beta}(\psi + y) - \mu b(\varepsilon^{-1} - \hat{\beta}\psi) + (1 - \mu b)\varepsilon^{-1} F_1, \tag{14a}$$

$$p = \psi - \tfrac{1}{2}\hat{\beta}\varepsilon\psi^2 + \varepsilon[\tfrac{1}{2} - \tfrac{1}{2}(u^2 + v^2)] + F_2, \tag{14b}$$

where

$$F_1 = -E_k \int_{-\infty}^{x} D^{-3}\left[K_2\left(\frac{\partial^2\psi}{\partial x^2} - 2D^{-1}\frac{\partial\psi}{\partial x}\frac{\partial D}{\partial x}\right) + \frac{\partial\psi}{\partial x}\frac{\partial K_2}{\partial x} + K_1\left(\frac{\partial^2\psi}{\partial y^2} - 2D^{-1}\frac{\partial\psi}{\partial y}\frac{\partial D}{\partial y}\right) + \frac{\partial\psi}{\partial x}\frac{\partial K_1}{\partial y}\right] \mathrm{d}x, \tag{15a}$$

$$F_2 = -E_k \int_{-\infty}^{x} [D^{-1}(K_1 u^2 + K_2 v^2) - K_1 u]\,\mathrm{d}x, \tag{15b}$$

Note that the first term on the right-hand side of eq. (14a) says the beta effect enhances existing negative (positive) vorticity when $\psi + y$ is positive (negative). The second term is dependent on the topographical parameter μ and varies inversely with the Rossby number except for very large values of ε when a small beta influence is possible. Note that far away from the topographical feature the integrand is zero provided conditions (6c–h) are satisfied. As previously indicated for mesoscale flow ($L = 10^5$ m) and mesoscale mountains the effect of $\hat{\beta}$ ($\hat{\beta} = \beta L^2 U^{-1}$) is minimal and is disregarded in this study.

Substituting from eqs. (9a,b,c) into (14a) for ζ, u and v yields an elliptical equation in ψ, namely,

$$\nabla^2\psi = \frac{\partial(\ln D)}{\partial x}\frac{\partial\psi}{\partial x} + \frac{\partial(\ln D)}{\partial y}\frac{\partial\psi}{\partial y} - \mu b D\varepsilon^{-1} + D^2\varepsilon^{-1}F_1, \tag{16}$$

which together with boundary conditions, eq. (6f), represents a boundary value problem. When $E_k = 0$, the resulting equation describes steady inviscid flow, see Bannon (1980) for a discussion of this flow past a topographical feature. When the fluid is viscous the numerical approach to determine ψ uses an iterative procedure. The inviscid solution is the first guess and the elliptical equation, (16), is then repeatedly solved with the integral term evaluated using the previous known solution. This process continues till convergence is achieved. For the ratio of $E_k K/\varepsilon$ much less than one there is no difficulty in obtaining convergence. Other details include the fact that the grid is 100 × 100 on which the topographical feature is centered and the grid spacing is 0.2. The integral expression is evaluated numerically by the trapezoidal rule.

To measure the influence of the topography upon the flow the following expressions are introduced (Bannon, 1980):

(Normalized Ekman drag)

$$C_{Ei} = \hat{C}_{Ei}/C_N, \qquad i = 1, 2, \tag{17a}$$

where

$$\hat{C}_{E1} = \hat{\delta}\gamma_R \iint u\,\mathrm{d}x\,\mathrm{d}y, \tag{17b}$$

$$\hat{C}_{E2} = \hat{\delta}\gamma_R \iint v\,\mathrm{d}x\,\mathrm{d}y, \tag{17c}$$

$$C_N = \hat{\delta}\gamma_R \iint u_\infty(y)\,\mathrm{d}x\,\mathrm{d}y; \tag{17d}$$

(Normalized topographical drag)

$$C_{\mathrm{T}i} = \hat{C}_{\mathrm{T}i}/C_N, \qquad i = 1, 2, \tag{18a}$$

where

$$\hat{C}_{\mathrm{T1}} = \hat{\delta}\mu \iint p\, \partial b/\partial x \,\mathrm{d}x\, \mathrm{d}y, \tag{18b}$$

$$\hat{C}_{\mathrm{T2}} = \hat{\delta}\mu \int p\, \partial b/\partial x \,\mathrm{d}x\, \mathrm{d}y, \tag{18c}$$

here $\hat{\delta}$ is the vertical aspect ratio;
(Blocking efficiency)

$$B(y) = 1 - \frac{F^+(0, y) + F^-(0, y)}{F^+(-\infty, y) + F^-(-\infty, y)}, \tag{19a}$$

where the zonal mass flux is

$$F^{\pm}(x, y) = \pm \int_0^{\pm y} u(x, \eta)\, D(x, \eta)\, \mathrm{d}\eta; \tag{19b}$$

(Asymmetry)

$$A(y) = \frac{F^+(0,y)/F^+(-\infty,y)}{F^-(0, y)/F^-(-\infty, y)} - 1. \tag{20}$$

Note that $B(\infty) = 0$, $A(y) = 0$ for symmetric flow and that $C_{\mathrm{T1}} + C_{\mathrm{E1}} \geqslant 1$ indicates the total drag is equal to or greater than that obtained without the obstacle.

3. Discussion of results

To assess the accuracy of the Oseen approximation for the boundary value problem (BVP), solutions of eqs. (16) and (14b) were compared with steady-state solutions from the non-linear initial boundary value problem (IBVP) given in Bannon (1980). This comparison showed that the blocking is underestimated in the BVP solutions but otherwise the overall flow pattern and pressure field were nearly the same provided the flows did not possess excessive curvature.

In Table 1, various topographical measures for an f-plane with Rayleigh friction when $\gamma_{\mathrm{R}} \equiv a$, $b = 0$, $K_1 = K_2$ and $\mu = 0.261/2$ are given for a range of Rossby numbers. For Rossby numbers one and ten, representing flows more typical of mesoscale conditions, the left–right asymmetry is considerably reduced with respect to the case $\varepsilon \ll 1$. Additionally, the pressure pattern becomes more symmetric, consequently the topographical drags are near zero while the velocity deviates little from its upstream value giving an Ekman drag of nearly one. Also evident is the fact that the blocking efficiency remains unchanged provided the Rossby number and γ_{R} are kept at a constant ratio (Bannon, 1980). The impact of the frictional drag on barotropic flow over an isolated shallow obstacle appears slight under mesoscale conditions.

Solutions in Table 2 are when the topographical parameter is increased four-fold to $\mu = 0.522$ with a Rossby number of 1 and the drag coefficient is allowed to influence none, one, or both velocity

Table 1. *Topographical measures for a fixed ratio of $\gamma_{\mathrm{R}}/\varepsilon$ with $\mu = 0.261/2$*

$\gamma_{\mathrm{R}}/\varepsilon$	ε	γ_{R}	$B(1)$	$B(2)$	$A(1)$	$A(2)$	C_{T1}	C_{T2}	C_{E1}	$V_{\max}$
0.2	0.1	0.02	0.063	0.030	0.433	0.629	0.139	0.756	1.005	1.37
0.2	1.0	0.2	0.063	0.030	0.036	0.049	0.003	0.076	1.004	1.05
0.2	10	2.0	0.063	0.030	0.004	0.005	0.001	0.008	1.004	1.05

Table 2. *Topographical measures for Rayleigh and quadratic friction when $\mu = 0.522$ and $\varepsilon = 1$*

$\dfrac{E_k K_1}{\varepsilon}$	$\dfrac{E_k K_2}{\varepsilon}$	$B(1)$	$B(2)$	$A(1)$	$A(2)$	C_{T2}	C_{E1}	$V_{\max}$
0	0	0.222	0.100	0.193	0.302			1.46
0.2	0	0.300	0.146	0.137	0.205	0.285	1.008	1.31
0.2	0.2	0.299	0.145	0.105	0.155	0.276	1.010	1.29
0.2*	0.2*	0.301	0.146	0.073	0.111	0.276	1.010	1.26

* Quadratic friction.

components. Only small differences exist however between the case when both drag components are non-zero and when only one is non-zero. This is predominantly because v is very small for $\varepsilon = 1$. The largest impact exists in the change of the left-right asymmetry. Similar results are denoted by the last line in Table 2 which represents the topographical measures when the Rayleigh friction is replaced with the standard quadratic form. This conclusion agrees with the findings of Han et al. (1982). Overall the influence of friction increases the blocking, reduces the left–right asymmetry and decreases the maximum velocity (Bannon, 1980), but the range of these indicated changes are still small. The optimistic appraisal of the importance of friction inferred by Buzzi and Tibaldi (1977), for small Rossby number flow, is somewhat dubious for mesoscale flows.

For zonal flow, in the absence of topography, the antitriptic pressure component compatible with a constant drag coefficient is $P_0 = -\gamma_R x$, i.e., in eq. (7) $b = 0$ and $a = \gamma_R$. This large-scale pressure feature implies in eq. (1) that $\partial u'/\partial Z$, at $Z = \mu b$, has a positive sign everywhere. From eqs. (6a), (6g) and (5d) it is clear that a change in the sign of $\partial P_0/\partial x$ means that $\partial u'/\partial Z$ must also change sign. In eq. (7) a theoretical mesoscale antitripic pressure trough ($b > 0$) or ridge ($b < 0$) like feature is introduced.

Solutions obtained using $a = 0.2$ and $b = 0.6$ with $\varepsilon = 1$ and $K_1 = K_2$ are displayed in Table 3 for a variety of mesoscale trough positions centered at $x = x_C$. When the trough is positioned at $x_C = -1$ or -2 just upstream of the obstacle centered at $x = y = 0$ its influence is to decrease the blocking yet increase the left–right asymmetry, the maximum velocity, and the normalized Ekman and topographical drags C_{E1} and C_{T2}, respectively, while C_{T1} is reduced. Note that $\partial P_0/\partial x$ is positive in this region thus K_1 and K_2 are negative over most of the obstacle. Consequently the barotropic flow is being forced, whenever F_1 and F_2 (eqs. 15a,b) are positive, because the obstacle has upset the antitriptic balance (F_1 will be displayed in Fig. 4). When centered downstream of $x = 0$, the trough acts to enhance the frictional drag and the blocking coefficients are consequently larger while the left-right asymmetry is decreased. Overall the influence of the trough feature is to greatly extend the range of the topographical measures.

Some of the solutions described in Table 3 are shown in Figs. 1a,b,c,d. Fig. 1a shows the no friction solution while Fig. 1b results from having constant Rayleigh friction, i.e., $a = 0.2$ and $b = 0$. Note that friction has reduced the velocities downstream from the topography. Fig. 1c corresponds to the case when the antitriptic pressure trough ($b = 0.6$, $a = 0.2$) is centered at $x_C = 1$ while Fig. 1d is the case when the same trough is centered at $x_C = -1$. Substantial velocity reductions occur downstream when $x_C = 1$ while the decreased velocities are upstream from the topography when $x_C = -1$. The dip in the calculated barotropic pressure p, solid line Figs. 1, over the obstacle can be explained by Bernoulli's theorem and is due to the increased flow speed (Bannon, 1980).

The differences in the above figures are highlighted even more in the vorticity profiles shown in Figs. 2a,b,c,d. For no friction, Fig. 2a, negative vorticity exists over the obstacle while with constant friction, Fig. 2b, the negative vorticity is slightly reduced in magnitude and positive vorticity

Table 3. *Topographical measures for $\varepsilon = 1$ and $\mu = 0.522$; the antitriptic pressure gradient, eq. (7), contains $a = 0.2$, $b = 0.6$ and x_c is allowed to vary as indicated*

x_c	$B(1)$	$B(2)$	$A(1)$	$A(2)$	C_{T1}	C_{T2}	C_{E1}	V_{max}
−2	0.243	0.108	0.131	0.191	0.043	0.293	1.034	1.39
−1	0.188	0.079	0.138	0.202	0.021	0.319	1.054	1.53
0	0.323	0.159	0.117	0.174	0.051	0.285	1.004	1.27
1	0.370	0.193	0.073	0.112	0.072	0.247	0.977	1.20
2	0.322	0.162	0.075	0.109	0.073	0.257	0.996	1.24
4	0.299	0.144	0.101	0.148	0.062	0.274	1.011	1.28
∞	0.299	0.145	0.105	0.155	0.058	0.276	1.010	1.29
no friction	0.222	0.100	0.193	0.302				1.46

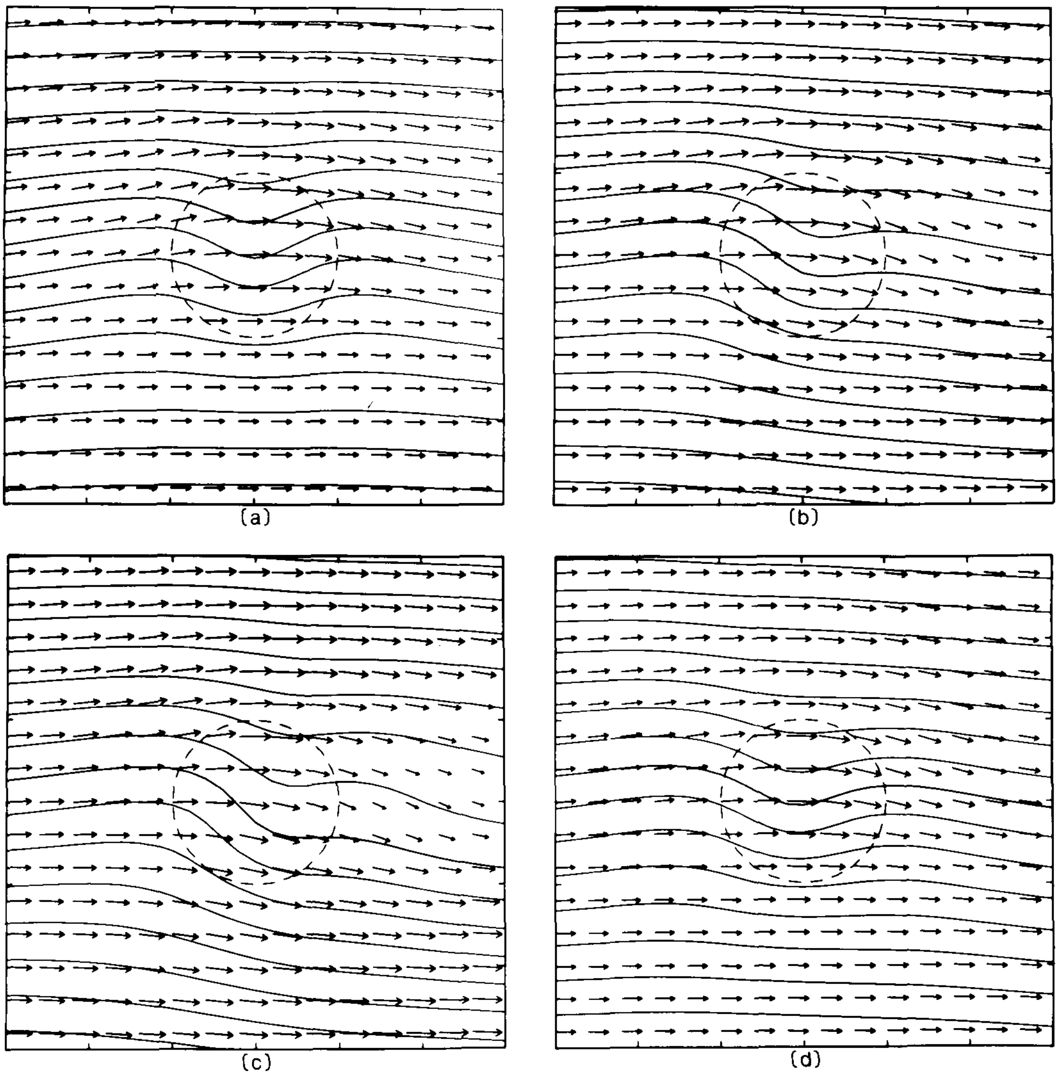

Fig. 1. Velocity vector field and pressure contours computed for $\varepsilon = 1$, $\mu = 0.522$ and $K_1 = K_2$. (a) $a = b = 0$ (eq. 7). (b) $a = 0.2$, $b = 0$. (c) $a = 0.2$, $b = 0.6$, $x_c = 1$. (d) $a = 0.2$, $b = 0.6$, $x_c = -1$. The contour interval for the non-dimensional pressure p is 0.4. The topography contour (dashed circle), of unit radius, is for half its maximum value.

is generated. Note how the vorticity couplet is enhanced when the trough is centered at $x_c = 1$ in Fig. (2c) while the positive vorticity is reduced and rotated counterclockwise when the trough is centered at $x_c = -1$ as shown in Fig. 2d.

Table 4 shows topographical measures when the constant frictional drag has been removed, i.e., $a = 0$ in eq. (7), but the mesoscale feature retained with $b = 0.6$ (set A) or $b = 0.4$ (set B). Clearly evident is the large range of values for the blocking and other measures. In set A (set B) the maximum antitriptic pressure gradient is equivalent to 0.3 (0.2) of a millibar in a distance L. Set B is computed with $K_2 = 0$. The pattern is similar with set A but since b is reduced by one-third the range of the topographical measures is equivalently reduced. Only minor differences occur in solutions obtained using $K_2 = 0$, $K_2 = K_1$ or K_2 a constant, (not shown), analogous with the results presented in Table 2.

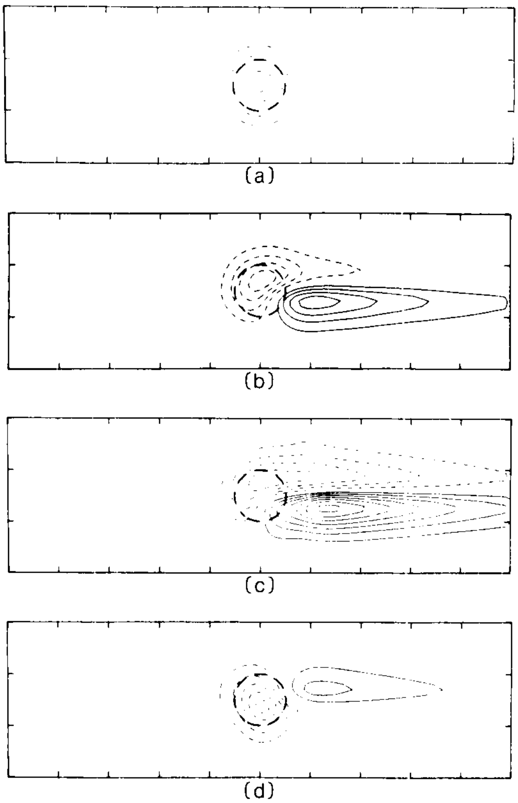

Fig. 2. Same as Fig. 1 except for vorticity. The contour interval is 0.1 and the zero contour is removed. Positive vorticity plotted as solid lines while negative is dashed.

The measures in Table 4 for $x_C = 1$, set B, are comparable with results computed with constant friction given in Table 2. In both, the maximum antitriptic pressure gradient is identical. However, in the former K_1 is a function of x, thus, only a small portion of the lee side is experiencing an equivalent frictional drag while the remainder is subjected to less. It appears that an isolated mesoscale feature strategically positioned can have as much influence as a larger scale feature.

To visualize what is happening to the fluid when the antitriptic pressure trough (ridge) is upstream (downstream) from the topography yet within its influence, Fig. 3a is presented showing the streamfunction for set B when $x_C = -1$. Note how the streamlines indicate confluence on the lee side of

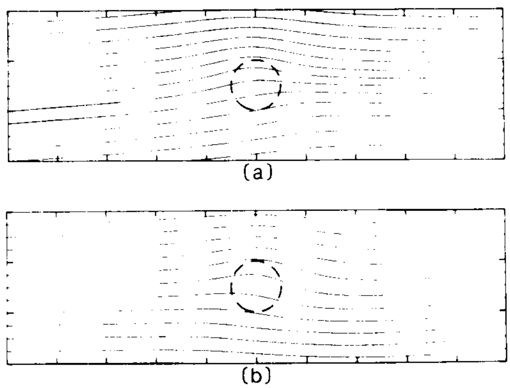

Fig. 3. Contours of the streamfunction for $\varepsilon = 1$ and $\mu = 0.522$. (a) $a = K_2 = 0$, $b = 0.4$ and $x_C = -1$. (b) $K_1 = K_2$, $a = 0.2$ and $b = 0$. In (a) the downstream boundary condition is $\partial\psi/\partial x = 0$. The contour interval is 0.5.

Table 4. *Topographical measures for $\varepsilon = 1$ and $\mu = 0.522$ when the antitriptic pressure gradient, eq. (7), contains $a = 0$, $b = 0.6$ (set A) or $b = 0.4$ (set B) and x_c* is allowed to vary as indicated

x_c	$B(1)$	$B(2)$	$A(1)$	$A(2)$	C_{T2}	C_{T1}	C_{E1}	V_{max}
(set A)								
−1	0.028	−0.020	0.214	0.347	0.372	−0.079	1.134	2.03
0	0.269	0.128	0.181	0.290	0.309	0.000	1.025	1.38
1	0.340	0.182	0.145	0.226	0.265	0.033	0.977	1.27
(set B)								
−1*	0.085	0.012	0.207	0.330	0.352	−0.045	1.106	1.81
0*	0.246	0.112	0.176	0.276	0.307	0.000	1.035	1.41
1*	0.302	0.154	0.170	0.261	0.201	0.025	0.997	1.33

* $K_2 = 0$.

the obstacle consequently the barotropic flow will tend to wrap itself somewhat around the topography. These characteristics are clearly different than the pattern exhibited on the lee side shown in Fig. 3b for a solution obtained with a constant surface drag, i.e., $a = 0.2$ and $b = 0$. As noted earlier the maximum antitriptic pressure gradient magnitudes are identical in both cases. Additionally Fig. 3a has been computed using the Neumann condition $\partial\psi/\partial x = 0$ at the downstream boundary. An identical solution is obtained, except right next to the downstream boundary, when the Dirichlet boundary condition $\psi = -y$ is used (not shown). Larger Rossby number flow (e.g. $\varepsilon = 4$) for $x_c = -1$, displays nearly an identical lee side flow pattern with confluence, but maintains better the zonal flow upstream of the obstacle.

Shown in Fig. 4a is the distribution of F_1 (eq. (15a)) associated with the antitriptic pressure trough and confluent flow described above. On the lee slopes F_1 is positive (solid lines) on the right side, when looking downstream, and negative (dashed lines) on the left. This pattern of negative forcing to the north of a region of positive forcing is consistent with the vorticity forcing requirements established in Pierrehumbert and Malguzzi (1984). A distribution similar to the above occurs when an antitriptic pressure ridge is placed on the lee side of the topography. Consequently the topographical measures are almost identical (not shown). This same pattern, but with diminished magnitude, is shown in Fig. 4b for the case when the antitriptic pressure trough is positioned on the lee side ($x_c = 1$). Localization of the pressure trough guarantees the finiteness of the sum of the forcing, i.e., F_1 is bounded as required (Pierrehumbert and Malguzzi, 1984).

It should be noted that under either forced or frictionally damped conditions the depth averaged flow can become barotropically unstable. This destabilization process occurs predominantly on the lee side under forced barotropic flow and is generated, e.g., by the jet like feature associated with the lee side confluence described above. In Fig. 5 the distribution of $\partial^2 u/\partial y^2$ is shown for set B with the antitriptic trough centered at $x_c = -1$. The lee side shows large magnitudes, negative over the center of the jet with a sign change clearly implying the condition for barotropic instability is more than satisfied. In reality, the lee side flow pattern predicted here under steady state conditions may

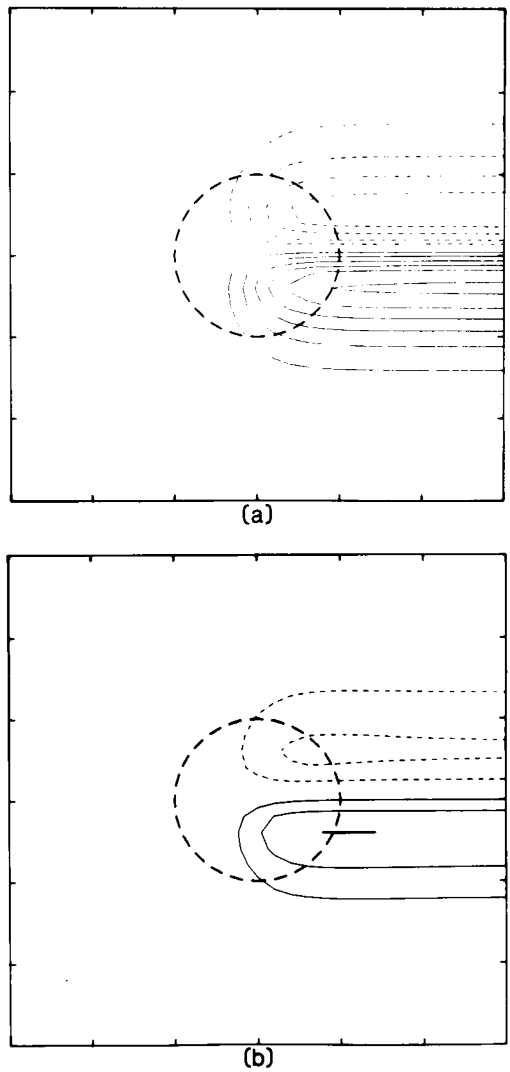

Fig. 4. Contours of F_1 (Eq. 15a). (a) $a = K_2 = 0$, $b = 0.4$ and $x_c = -1$ (antitriptic pressure trough on upwind slope). (b) $a = K_2 = 0$, $b = 0.4$ and $x_c = 1$ (antitriptic pressure trough on lee slope). Contour interval is 0.15 and zero contour removed. Positive values plotted as solid lines while negative is dashed. Note that F_1 is the integral with respect to x of the forcing and damping terms on the right side of eq. (8a).

never fully develop, because, of the development associated with the barotropic instability which will broaden and weaken a narrow jet (Pedlosky, 1979, p. 511). The time and spacial scale of the latter is completely determined by the characteristics of the mean flow. Applying our scaling to Emanuel's

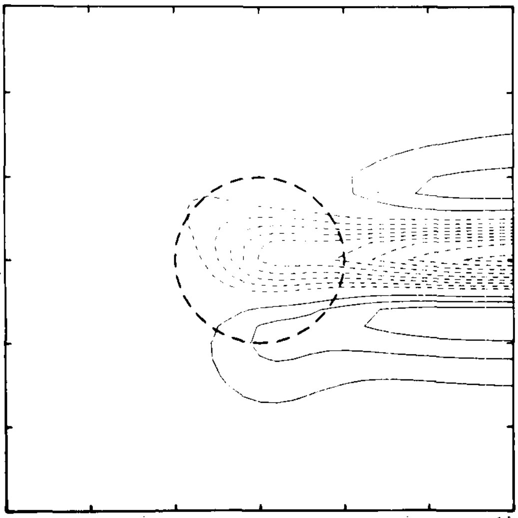

Fig. 5. Contours of $\partial^2 u/\partial y^2$ for case (a) in Fig. 4. Contour interval is 0.3 and zero contour is not included. Positive values plotted as solid lines while negative is dashed.

(1983) barotropic stability criteria yields a predicted horizontal scale proportional to $L(10^5$ m) with the time scale related to $(\partial U/\partial y)^{-1}$ yielding LU^{-1} $(10^4$ s). However, similar horizontal and time scales are predicted by baroclinic instability (Emanuel, 1983), provided the Richardson number is of order unity. This is the case during the early rapid growth stage of lee cyclogenesis (Buzzi and Tibaldi, 1978). Thus barotropic and baroclinic processes are difficult to separate since both imply a conversion from the mean to a perturbation of the same scale.

Additionally our model predicts that the total and perturbation barotropic kinetic energies are largest when the trough feature is on the upwind side of the obstacle. For the total region investigated the perturbation kinetic energy is twice as large when $x_C = -1$ (upwind slope) as compared to the results when the trough is located on the lee slope ($x_C = 1$), while the total kinetic energy shows a similar trend. This may explain, in part, the decline in the barotropic contribution after the peak which occurs while the front is yet on the upwind side of the topography (Tibaldi et al., 1980). Also, the lee side jet may be associated with the strong low level ageostrophic downslope winds that precedes the rapid lee development (McGinley, 1982).

Basically the reaction of the linear barotropic flow to localized forcing and damping must be classified as a low amplitude response (no closed streamlines). The possibility of a high amplitude response (closed streamlines) in a non-linear regime for internally generated forcing and damping (Pierrehumbert and Malguzzi, 1984) remains to be tested.

4. Conclusions

Mesoscale flow over an isolated topographical feature in a rotating barotropic fluid having an antitriptic balanced background state is studied. Localized internally generated forcing and damping results when the background state is disrupted by the obstacle. The greatest forcing occurs when an idealized antitriptic pressure trough is positioned on the upwind slope. Both the mean and the perturbation kinetic energy are a maximum at this time. An important finding is that when the barotropic flow is forced, the topographically disturbed flow responds by reducing the blocking and generating a confluent flow pattern on the lee side. The enhanced depth averaged winds on the lee side may be associated with strong downslope winds that precede rapid lee development and may lead to barotropic instability. In this study this occurs when an antitriptic pressure trough exists on the upwind side or a ridge on the lee side. The enhanced confluence is found to be maintained even for large Rossby numbers, e.g., $\varepsilon = 4$. When the center of the antitriptic pressure trough (ridge) is slightly downstream (upstream) of the topography, then increased blocking occurs along with an enhanced vorticity couplet. A mesoscale feature, in our case the antitriptic balanced state, located predominately on one side or the other of the topography is shown to have a significant influence. The impact from barotropic flow interacting with topography should clearly be enlarged, as shown here, when both frictional drag and (baroclinic) forced conditions are considered.

5. Acknowledgements

The author thanks Professor Peter Bannon of the University of Chicago for fruitful discussions and for providing some computing resources under

National Science Foundation Grant ATM 80–26790. This work was completed by the author while at the University of Wisconsin and is based upon work supported by the National Science Foundation under Grant DPP-8119155. Computing resources used in this research are supported by the National Center for Atmospheric Research (NCAR) which is sponsored by the National Science Foundation. I thank Eva M. Singer for skilfully typing this manuscript.

REFERENCES

Bannon, P. R. 1980. Rotating barotropic flow over finite isolated topography. *J. Fluid Mech. 101*, 281–306.

Barry, R. G. 1981. *Mountain weather and climate.* Methuen, 313 pp.

Buzzi, A. and Tibaldi, S. 1977. Inertial and frictional effects on rotating and stratified flow over topography. *Q. J. R. Meteorol. Soc. 103*, 135–150.

Buzzi, A. and Tibaldi, S. 1978. Cyclogenesis in the lee of the Alps: a case study. *Q. J. R. Meteorol. Soc. 104*, 271–287.

Charney, J. G. 1955. The gulf stream as an inertial boundary layer. *Proc. Natl. Acad. Sci. 41*, 731–740.

Emanuel, K. A. 1983. On the dynamical definition(s) of "mesoscale", In *Mesoscale Meteorology—Theories, Observations and Models*, Lilly, D. K. and T. Gal-Chen, eds. Reidel Pub. Co., Dordrecht, Holland, 1–11.

Haltiner, G. J. and Williams, R. T. 1980. *Numerical prediction and dynamic meteorology.* John Wiley & Sons, 477 pp.

Han, Y. J., Ueyoshi, K. and Deardorff, J. W. 1982. Numerical study of terrain-induced mesoscale motions in a mixed layer. *J. Atmos. Sci. 39*, 2464–2476.

Houghton, D. D. and Kasahara, A. 1968. Nonlinear shallow fluid flow over an isolated ridge. *Comm. Pure Appl. Math. 21*, 1–23.

Hoxit, L. R. 1974. Planetary boundary layer winds in baroclinic conditions. *J. Atmos. Sci. 31*, 1003–1020.

Huppert, H. E. and Stern, M. E. 1974. The effect of side walls on homogenous rotating flow over two-dimensional obstacles. *J. Fluid Mech. 64*, 417–436.

Kalnay-Rivas, E. and Merkine, L. 1982. A simple mechanism for blocking. *J. Atmos. Sci. 38*, 2077–2091.

Keyser, D. and Anthes, R. A. 1977. The applicability of a mixed-layer model of the planetary boundary layer to real-data forecasting. *Mon. Wea. Rev. 105*, 1351–1371.

Keyser, D. and Anthes, R. A. 1982. The influence of planetary boundary layer physics on frontal structure in the Hoskins–Bretherton horizontal shear model. *J. Atmos. Sci. 39*, 1783–1802.

Kurihara, Y. and Bender, M. A. 1983. A numerical scheme to treat the open lateral boundary of a limited area model. *Mon. Wea. Rev. 111*, 445–454.

Lavoie R. L. 1974. A numerical model of trade wind weather on Oahu. *Mon. Wea. Rev. 102*, 630–637.

Mahrt, L. J. 1974. Time-dependent, integrated planetary boundary layer flow. *J. Atmos. Sci. 31*, 457–464.

McGinley, J. 1982. A diagnosis of alpine lee cyclogenesis. *Mon. Wea. Rev. 110*, 1271–1287.

Pedlosky, J. 1979. *Geophysical fluid dynamics.* Springer-Verlag, New York, 624 pp.

Pierrehumbert, R. T. and Malguzzi, P. 1984. Forced coherent structures and local multiple equilibria in a barotropic atmosphere. *J. Atmos. Sci. 41*, 246–257.

Smith, R. B. 1982. Synoptic observations and theory of orographically disturbed wind and pressure. *J. Atmos. Sci. 39*, 60–70.

Stevenson, J. W. and Janowitz, G. S. 1977. The effect of Ekman suction on a flow over a shallow topography in the beta plane. *Dyn. Atmos. Oceans 1*, 225–239.

Taylor, G. I. 1915. Eddy motion in the atmosphere. *Phil. Trans R. Soc. London A215*, 1–26.

Tibaldi, S., Buzzi, A. and Malguzzi, P. 1980. Orographically induced cyclogenesis: Analysis of numerical experiments. *Mon. Wea. Rev. 108*, 1302–1314.

Tosi, E., Fantini, M. and Trevison, A. 1983. Numerical experiments on orographic cyclogenesis: Relationship between the development of the lee cyclone and the basic flow characteristics. *Mon. Wea. Rev. 111*, 799–814.